Numerical Simulation of Liquid Injection into an Anisothermal Dense Fluidized Bed

A. Ozel[1,2], A. Sarthou[1,2], Z. Zeren[1,2], P. Fede[1,2], O. Simonin[1,2],
I. Ghouila[3] and J.-L. Chamayou[3]

[1] *Université de Toulouse; INPT, UPS; IMFT; 31400 Toulouse, France*
[2] *CNRS; Institut de Mécanique des Fluides de Toulouse; 31400 Toulouse, France*
[3] *Ineos Chemicals Lavéra SAS, Centre de Technologie, BP6-13117 Lavéra - France*

Keywords: Two-fluid model, fluidized bed, evaporation, liquid injection

Abstract

Fluidized beds are widely used in reactive industrial processes such as: olefins production, oil cracking or uranium fluorination because of their high efficiency mixing properties. In such processes, the chemical reaction is strongly dependent on the temperature and liquid is injected into the reactor in order to cool it. The experimental data of the time evolution of the gas temperature in an anisothermal dense fluidized bed with a liquid injection provided by INEOS is first compared with the results predicted by a simple model with an assumption of a perfectly mixed fluidized bed (uniform solid and temperature distribution in the bed). The results of this simple model show that the time evolution of the gas temperature is accurately predicted. Additionally, we point out that the wall-to-bed heat transfer plays a crucial role of the gas temperature in the bed. Then, we performed 3-D numerical simulations that let us investigate local interactions between phases and heat transfer with wall. The simulations show that the liquid evaporates quickly and the temperature is in a satisfactory agreement with the experiment data.

Nomenclature

Symbols

d_p / d_l	Particle/Droplet diameter
α_k	Volume fraction of phase k
$U_{k,i}$	Mean velocity of phase k
$V_{r,i}$	Mean relative velocity between gas and dispersed phases
H_k	Enthalpy of phase k
T_k	Temperature of phase k
Y_{vap}	Liquid vapour mass fraction
χ_d	Number of density of droplets
Γ_l	Interfacial mass transfer
$I_{g\to k}$	Mean drag force (gas to dispersed phase)
$\Sigma_{k,ij}$	Effective stress tensor of phase k
λ_k	Bulk viscosity of phase
μ_k	Viscosity of phase k
P_g	Gas pressure
g_i	Gravity
q_k^2	Dispersed phase agitations
τ_{gp}^F	Characteristic relaxation time scale
τ_{gl}^T	Characteristic convection/diffusion heat transfer time scale
$V_{d,i}$	Drift velocity
Re_p	Reynolds number
$Sh / Sc / B_M$	Sherwood/Schmidt/Spalding number

Subscripts

g	Gas phase
p	Particle phase
l	Liquid phase

Introduction

Gas-liquid-solid fluidized beds are extensively used for chemical, petrochemical and biochemical processing such as the fluid catalytic cracking, the production of polyethylene. The liquid is injected into the reactor and evaporates through the bed with a reaction in order to control bed temperature. The main advantage of the liquid injection is the reduction of operational cost as compared with a process using external heat exchangers to cool down the bed. A detailed knowledge about the mechanism of liquid injection into fluidized bed reactors is required for the

safety reasons of the industrial processes as well.

The liquid injection into an anisothermal fluidized bed has been experimentally investigated by the following studies: Ariyapadi et al. (2003) used Digital X-ray Technique to determine the liquid jet expansion and the penetration into a bed. In this study, ethanol was introduces into a bed of fluid catalytic cracking (FCC) catalyst particle. House et al. (2004) showed that liquid droplets form just below the jet plume and proposed a simple model to determine the effect of liquid-solid mixing and heat transfer on products. Bruhns and Werther (2005) studied the agglomeration of water/ethanol with FCC catalyst/sand and large-scale particle mixing in a pilot-scale bubbling fluidized by using the same experimental technique. From the point of view of the multi-phase flow modeling, the empirical models are mainly employed for the liquid injection into a fluidized bed due to their simplicity. Such empirical models are useful for the conceptual design of fluidized bed where the design parameters could be tested rapidly. Kunii and Levensiel (1991) summarized several empirical correlations for bed hydrodynamics, the heat transfer and dispersion coefficients. However, empirical models cannot take into account the local interactions and inhomogenities in a bed. At this point, the numerical simulations by using the multi-fluid or Eulerian-Eulerian approach supplies further information about in the fluidized bed. In the framework of the Eulerian-Eulerian approach, the phases are modeled with an assumption of interpenetra continuum supplemented by Kinetic Theory of Granular Flow (KTGF).

In the present work, we first use a simple model to predict the time evolution of the temperature in a gas-liquid–solid fluidized bed with taking into account the wall-to-bed heat transfer. This model allows us to rapidly test the different parameters of heat transfer modeling. Then, we performed a numerical simulation of gas-liquid solid fluidized bed by using the Eulerian-Eulerian modeling approach developed by Simonin (1991) to investigate the local interaction between phases. This approach has been already extensively used to predict various types of dilute and dense multi-phase flows, such as: turbulent round jets: (Simonin, 1991), particle-laden confined flows (He and Simonin, 1993), fluidized beds (Balzer et al., 1995 and Gobin et al., 2003), uranuium flouration (Konan, 2010). This model not only accounts for particle–particle collisions but also for the drag-induced effects of the interstitial fluid. An Eulerian n-fluid modelling approach for fluid-particle turbulent polydispersed flows implemented by IMFT (Institut de Mécanique des Fluide de Toulouse) in the *NEPTUNE_CFD v1.08@Tlse* version. *NEPTUNE_CFD* is a multiphase flow software developed in the framework of the NEPTUNE project, financially supported by CEA (Commissariat à l'Energie Atomique), EDF (Electricité De France), IRSN (Institut de Radioprotection et de Sûreté Nucléaire) and AREVA-NP (see for the parallezation efficiency of the code, Neau et al. (2010)).

Experimental Facility

The experimental study was conducted by INEOS. The geometry is a pilot-scale fluidized bed with a dome mounted at the top (see Figure 1). A mixture of nitrogen and n-hexane with the temperature $99C^o$ fluidized the solid phase. Then, liquid pentane with a lower temperature was injected at the specific height during $60s$. The density and viscosity of the fluidization gas is $18kg/m^3$ and $1.95\times10^{-5}Pa.s$, respectively. The solid mass of the bed is $510kg$ and particles are of a diameter of $550-650\mu m$. The density of solid particle is $750-850kg/m^3$ and the density of liquid pentane is around $600kg/m^3$. The specific heat capacity of the fluidization gas, solid particles, liquid pentane and pentane vapour is of $1372, 2000, 2438, 2921J/kgK$, respectively. During the experiment, the gas temperature was recorded at several locations of the fluidized bed.

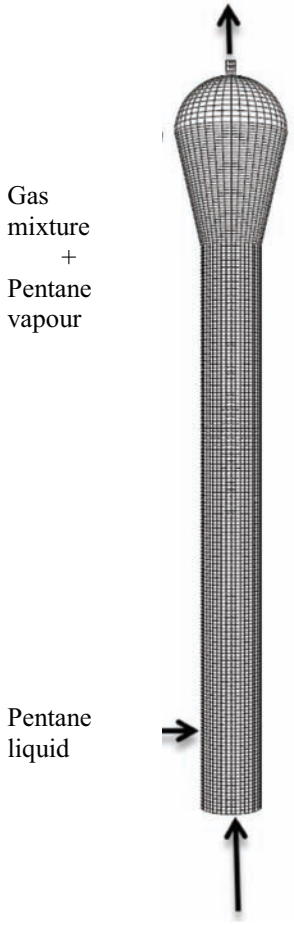

Figure 1. The fluidized bed geometry

A Simple Model

To determine the time evolution of the gas temperature in the bed, a simple model is first proposed with a few assumptions. The temperature and solid phase distribution is uniform in the bed ($T_b = T_g = T_p$ where T_b is the bed temperature and g refers to the gas phase, l refers to solid phase and p refers to the solid phase). The evaporation occurs with infinite reaction rate and there is no reaction of

the solid phase. The heat balance in the bed reads:

$$\frac{dE_{bed}}{dt} = c_{p,g}T_b\dot{m}_g + \left(c_{p,l}T_b - L_{vap}\right)\dot{m}_l + c^*_{p,g}T_b\dot{m}_{out} + h_{wall}S_{wall}(T_w - T_b)$$

The first term on the left-hand side represents the energy supplied by the fluidization gas. The second term is the energy transfer between the gas phase and liquid pentane due to the evaporation. The third one is the energy that leaves the bed and the last term is the heat flux between the wall and the bed. E_{bed} is the total energy in the bed, $\dot{m}_g$, $\dot{m}_l$ and $\dot{m}_{out}$ are the mass flux of the fluidization gas, liquid pentane and at the bed outlet, respectively. T_b and T_w are the bed and the wall temperature, L_{vap} is latent heat of vaporization of liquid pentane, $c_{p,g}$ and $c_{p,l}$ are the specific heat capacity of the fluidization gas and the liquid. S_{wall} is the total surface of the wall and h_{wall} is the heat transfer coefficient between the bed and the wall. The gas mixture specific heat $c^*_{p,g}$ is given by

$$c^*_{p,g} = c_{p,g}(1 - Y_{vap}) + c_{p,vap}Y_{vap}$$

with the mass fraction of the liquid vapor Y_{vap} defined as

$$Y_{vap} = \frac{\dot{m}_l}{\dot{m}_l + \dot{m}_g} - \exp\left[-\frac{\dot{m}_l + \dot{m}_g}{m_g T_b}\right]\frac{\dot{m}_l}{\dot{m}_l + \dot{m}_g}.$$

where m_g is the total gas mass in the bed. The temperature of the bed T_b is calculated by

$$T_b = \frac{E_{bed}}{m_g c^*_{p,g} + m_p c_{p,p}}.$$

A sketch of the bed wall is illustrated in Figure 1. We assume that the glass wool of the wall is adiabatic. The heat transfer coefficient $h_w[W/m^2K]$ must be modeled in terms of many factors such as the particle properties, the wall emissivity or the bed solid concentration. We tested the different boundary conditions and the heat transfer coefficient for the wall to investigate the effect of the heat transfer due to the wall on the cooling of the bed. The results are given in the last section.

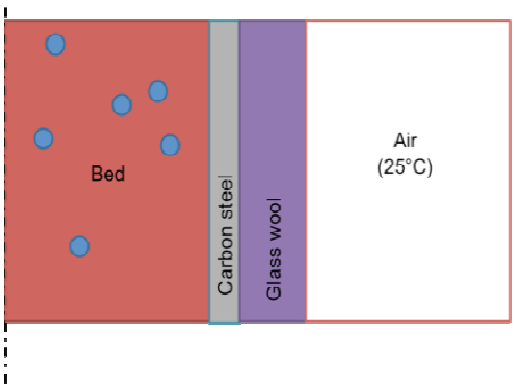

Figure 2: The schematic view of the wall.

Multi-Fluid Eulerian Approach

The modeling approach is based on the multi-fluid model formalism that involves mean separate transport equations of mass, momentum and energy for continuum phase (gas) and dispersed phases (particles and droplets). Interactions between phases are coupled through inter-phase transfers. The modified two-equation turbulence model (turbulent kinetic and dissipation energy) that takes into account effects of dispersed phase is used to solve gas-phase turbulence. Two transport equations, developed in the frame of kinetic theory of granular media supplemented by the interstitial fluid effect and the interaction with the turbulence (Balzer et al., 1996), are resolved to model the effect of velocity fluctuations and inter-particle collisions on the dispersed phase hydrodynamic. Concerning the transfers between the phases with reactive flow, we do not account for the heat transfer between particles and droplets. The drag force and the momentum transfer due to evaporation were taken into account for between gas and liquid phase. The drag force was accounted for the particulate phase and the gas phase. The gas density varies with the temperature and it is assumed that the droplets have monodisperse distribution with evolution of the diameter during the evaporation. The specific heat capacity of the gas is independent of the temperature and it is a function of the local concentration of the liquid vapor.

Mass and Momentum Balance Equations

The multi-fluid mass balance equation for the each phase is written

$$\frac{\partial}{\partial t}\left(\alpha_g\rho_g\right) + \frac{\partial}{\partial x_i}\left(\alpha_g\rho_g U_{k,i}\right) = -\Gamma_l$$

$$\frac{\partial}{\partial t}\left(\alpha_l\rho_l\right) + \frac{\partial}{\partial x_i}\left(\alpha_l\rho_l U_{k,i}\right) = \Gamma_l$$

$$\frac{\partial}{\partial t}\left(\alpha_p\rho_p\right) + \frac{\partial}{\partial x_i}\left(\alpha_p\rho_p U_{k,i}\right) = 0$$

with Γ_l is the mass transfer between liquid and gas phase. $\alpha_k\ \rho_p, U_{k,i}$ are the volume fraction, density and mean velocities of the phase k, respectively.

The momentum balance equation for the gas phase is

$$\frac{\partial}{\partial t}\left(\alpha_g\rho_g U_{g,i}\right) + \frac{\partial}{\partial x_j}\left(\alpha_g\rho_g U_{g,j}U_{g,i}\right) = -\alpha_g\frac{\partial P_g}{\partial x_i} + \alpha_g\rho_g g_i - \frac{\partial}{\partial x_j}\Sigma_{g,ij} + \sum_{k\neq g} I_{g\to k} + \Gamma_l(U_{\sigma,i} - U_{g,i})$$

and for the liquid phase

$$\frac{\partial}{\partial t}\left(\alpha_l\rho_l U_{l,i}\right) + \frac{\partial}{\partial x_j}\left(\alpha_l\rho_l U_{l,j}U_{l,i}\right) = -\alpha_l\frac{\partial P_g}{\partial x_i} + \alpha_l\rho_l g_i - \frac{\partial}{\partial x_j}\Sigma_{l,ij} + I_{l\to g} - \Gamma_l(U_{\sigma,i} - U_{,i}).$$

$U_{\sigma,i}$ represents the i^{th} component of the mean velocity of mass passing through the interface between the gas and the liquid phase. It is assumed to be equal to the mean liquid phase velocity $U_{l,i}$.

The momentum balance equation for the particulate phase is

$$\frac{\partial}{\partial t}\left(\alpha_p \rho_p U_{p,i}\right)+\frac{\partial}{\partial x_j}\left(\alpha_p \rho_p U_{p,j} U_{p,i}\right)=-\alpha_p \frac{\partial P_g}{\partial x_i}$$

$$+\alpha_p \rho_p g_i-\frac{\partial}{\partial x_j}\Sigma_{p,ij}+I_{p\to g}$$

with the mean gas pressure P_g, the acceleration due to the gravity g_i, the effective stress tensor $\Sigma_{k,ij}$, the mean drag force between the gas phase to the disperse phase $I_{g\to k}$.

Energy Balance Equations

The transport equation of the energy is considered for the total enthalpy. The enthalpy balance of the gas phase is

$$\frac{\partial}{\partial t}\left(\alpha_g \rho_g H_g\right)+\frac{\partial}{\partial x_i}\left(\alpha_g \rho_g H_g U_{g,i}\right)=-\frac{\partial}{\partial x_i}\left(\alpha_g \rho_g K_g \frac{\partial H_g}{\partial x_i}\right)$$

$$-\sum_{k\neq g}\left(\alpha_k \rho_k c_{p,k}\frac{T_g-T_k}{\tau_{gk}^T}\right)-\Gamma_l(H_\sigma-H_g)$$

and for the liquid phase

$$\frac{\partial}{\partial t}\left(\alpha_l \rho_l H_l\right)+\frac{\partial}{\partial x_i}\left(\alpha_l \rho_l H_l U_{l,i}\right)=-\frac{\partial}{\partial x_i}\left(\alpha_l \rho_l K_l \frac{\partial H_g}{\partial x_i}\right)$$

$$-\alpha_l \rho_l c_{p,l}\frac{T_l-T_g}{\tau_{gl}^T}+\Gamma_l(H_\sigma-H_g)$$

where H_σ is the transfer of the enthalpy from the liquid phase to the gas phase if there is evaporation or from the gas phase to the liquid phase if there is condensation. With an assumption, the reaction is directly released in the surrounding gas, the mean enthalpy passing through phase interface is set to the enthalpy of the evaporated liquid ($H_\sigma = H_l$).

The transport equation of enthalpy for the particulate phase is

$$\frac{\partial}{\partial t}\left(\alpha_p \rho_p H_p\right)+\frac{\partial}{\partial x_i}\left(\alpha_p \rho_p H_p U_{p,i}\right)=-\frac{\partial}{\partial x_i}\left(\alpha_p \rho_p K_p \frac{\partial H_p}{\partial x_i}\right)$$

$$-\alpha_l \rho_l c_{p,l}\frac{T_p-T_g}{\tau_{gl}^T}+\Phi_{reac}$$

The term Φ_{reac} is energy source term due to reaction such as polymerization, the heat exchanged during the particle-particle collision. We neglected the heat exchanged during the particle-particle collisions and there is no reaction between the gas and the particulate phase. The convection/diffusion heat transfer between the dispersed phases and the gas phase is modeled according to the following term:

$$\alpha_k \rho_k c_{p,k}\frac{T_k-T_g}{\tau_{gk}^T}$$

and K_k is the effective phase diffusivity in the enthalpy equations. The temperature of each phase is calculated by

$$H_g = c_{p,g}^*(T_g-T_g^0)$$

$$H_l = c_{p,l}(T_l-T_l^0)-H_l^0(T_l 0)$$

$$H_p = c_{p,p}^*(T_p-T_p^0)$$

T_g^0 is chosen as the reference temperature and then $H_{g,vap}(T_g^0)$ and $H_g(T_g^0)$ is equal to zero. $c_{p,k}$ is the specific heat of the phase k and the specific heat of gas $c_{p,g}^*$ is a function of the local concentration of liquid vapor calculated by

$c_{p,g}^* = Y_{vap}c_{p,vap}+(1-Y_{vap})c_{p,g}^0$.

Y_{vap} is the mass fraction of the liquid vapor and the transport equation of the mass fraction of the liquid vapor is given in the next section.

Evolution of The Droplet Sizes

The liquid vapor is dispersed in the gas phase by molecular (Fick's law) and turbulent motions. The transport equation of the mass fraction of the liquid vapor is

$$\frac{\partial}{\partial t}\left(\alpha_g \rho_g Y_{vap}\right)+\frac{\partial}{\partial x_i}\left(\alpha_g \rho_g Y_{vap} U_{g,i}\right)=-\frac{\partial}{\partial x_i}\left(\alpha_g \rho_g D_{vap}\frac{\partial Y_{vap}}{\partial x_i}\right)$$

$$+\Gamma_l Y_{vap}-\Gamma_l$$

where D_{vap} is the molecular diffusivity coefficient and it is equal to $1.3\times10^4\ kg/m.s$.

To determine the droplet size, we use the number χ_d of droplets per unit volume. With an assumption of spherical droplets, the number of droplets is

$$\chi_d = \frac{6}{\pi \rho_l d_l^3}.$$

We normalize the number of droplets X_d by the initial number of droplets:

$$\chi_d^* = \frac{\chi_d}{\chi_d^0}$$

The transport equation of χ_d^* is given by

$$\frac{\partial}{\partial t}\left(\alpha_l \rho_l \chi_d^*\right)+\frac{\partial}{\partial x_j}\left(\alpha_l \rho_l \chi_d^* U_{l,i}\right)=-\frac{\partial}{\partial x_i}\left(\alpha_l \rho_l D_{vap}^t \frac{\partial \chi_d^*}{\partial x_i}\right)$$

$$-\Gamma_l \chi_d^*$$

where D_{vap}^t is the diffusivity coefficient due to the transport by the liquid phase fluctuations. Then, we can obtain the diameter of the droplet by the following equation

$$d_l = \frac{d_l^0}{\chi_d^{*1/3}}$$

where d_l^0 is the initial droplet diameter. With an assumption of a ideal gas, the density of gas ρ_g is governed by

$$\rho_g = \frac{P_g W_g}{R_g T_g}$$

where W_g and R_g are the gas molar and the gas constant, respectively.

Interfacial Mass Transfer

The interfacial mass transfer term Γ_l is a function of the mass flux of the evaporated liquid and the number of droplets per unit mass n_l:

$$\Gamma_l = n_l \frac{dm_l}{dt}$$

where n_l is the number density of droplets given by $n_l = \alpha_l \rho_l \chi_d$ and $\frac{dm_l}{dt}$ represents the variation of the mass of the droplet. It is modelled as

$$\frac{dm_l}{dt} = -\pi d_l \rho_l D_{vap} Sh \ln(B_M)$$

with d_l, Sh, B_M are the droplet diameter, Sherwood and Spalding number. The Sherwood number is defined by the following correlation

$$Sh = 2 + 0.6 Re^{1/2} Sc^{1/3} \quad \text{if } Re\,Sc^{2/3} < 50000$$

with the Schmidt number $Sc = \frac{\mu_f}{\rho_g D_{vap}}$. The Spalding number takes into account the gradient of liquid vapor concentration from the droplet surface to the free-stream:

$$B_M = \frac{1 - Y_{vap}^{\infty}}{1 - Y_{vap}^{surf}}$$

Y_{vap}^{∞} and Y_{vap}^{surf} is the vapor concentration at the free-stream and the droplet surface, respectively. The mole fraction at the surface of the droplet is given by

$$X_{vap}^{surf} = exp\left[\frac{\Delta H_{vap} M_l}{R_g} \left(\frac{1}{T_{vap}} - \frac{1}{T_l^{surf}} \right) \right]$$

The liquid vapor concentration at droplet surface is proportional to the mole fraction at the surface as

$$Y_{vap}^{surf} = \frac{1}{1 + \frac{1 - X_{vap}^{surf}}{X_{vap}^{surf}} \frac{M_g}{M_l}}$$

with the molar mass of the liquid M_l and the gas M_g. The exchange of the enthalpy ΔH_{vap} is $\Delta H_{vap} = c_{p,vap}(T_l - T_l^0) - c_{p,l}(T_l - T_l^0) + H_l^0(T_l^0)$.

Interfacial Momentum Transfer

The mean drag force between the gas phase to the disperse phase k can be modeled as follows:

$$I_{g \to k} = -I_{k \to g} = \frac{\alpha_k \rho_k}{\tau_{gk}^F} V_{r,i}$$

with

$$\frac{1}{\tau_{gk}^F} = \frac{3}{4} \frac{\rho_g}{\rho_p} \frac{\langle C_D \rangle}{d_p} \langle | \mathbf{v}_r | \rangle.$$

τ_{gk}^F is the particle/droplet relaxation time scale, $\langle . \rangle$ is the ensemble average operator over the disperse phase (Simonin, 1996). The mean drag coefficient of a single particle/droplet $\langle C_d \rangle$ can be written as function of a particle Reynolds number and defined by Wen and Yu (1965) and Ergun correlation. The combination of two correlations was given by Gobin et al. (2003):

$$\langle C_D \rangle = \begin{cases} \min\left(\langle C_D^{Ergun} \rangle, \langle C_D^{Wen\&Yu} \rangle \right) & \text{if } \alpha_k > 0.3 \\ \langle C_D^{Wen\&Yu} \rangle & \text{if not} \end{cases}$$

where

$$\langle C_D^{Wen\&Yu} \rangle = \frac{24}{\langle Re_p \rangle} [1 + 0.15 \langle Re_p \rangle^{0.687}] \alpha_g^{-1.7}$$

and

$$\langle C_D^{Ergun} \rangle = 1.75 + \frac{150}{\langle Re_p \rangle}$$

with the definition of the mean particle Reynolds number $\langle Re_p \rangle = \alpha_g d_k \langle | \mathbf{v}_r | \rangle_p / \nu_g$ where d_p is the particle diameter and is the viscosity of gas, respectively. The term $\langle | \mathbf{v}_r | \rangle_p$ represents the local instantaneous relative velocity $v_{r,i}$ and is equal to difference between the local particle/droplet velocity $u_{k,i}$ and the instantaneous gas velocity $\tilde{u}_{g,i}$ which is undisturbed by presence of the particle/droplet at the particle position. $V_{r,i}$ is the averaged of the local relative velocity and equal to $\langle \tilde{u}_{g,i} - u_{k,i} \rangle$. It can be expressed in terms of the averaged velocity between phases and drift velocity $V_{d,i}$ due to the correlation between the instantaneous distribution of dispersed particles/droplets and the turbulence structure of gas phase: $V_{r,i} = U_{k,i} - U_{g,i} - V_{d,i}$. The drift velocity $V_{d,i}$ in the special case of particles suspended in homogeneous turbulence can be modeled (Deutsch and Simonin, 1991).

Turbulence Modeling

The effective stress tensor $\Sigma_{k,ij}$ consists of two parts for gas and dispersed phases; the molecular viscosity $\theta_{k,ij}$ and the Reynolds stress tensor $\langle u_{k,i}' u_{k,j}' \rangle$. The Reynolds stress tensor is modeled by using Boussinesq-like approximation with introducing the turbulent viscosity ν_g^t and the turbulent kinetic energy q_g^2 for the gas phase:

$$\langle u_{g,i}' u_{g,i}' \rangle = -\nu_g^t \left[\frac{\partial U_{g,i}}{\partial x_j} + \frac{\partial U_{g,i}}{\partial x_j} \right] + \frac{2}{3} \left[q_g^2 + \nu_g^t \frac{\partial U_{g,m}}{\partial x_m} \right]$$

The turbulent kinetic energy is defined by $q_g^2 = \frac{1}{2} \langle u_{g,i'} u_{g,i'} \rangle$ and the turbulent viscosity is given by Balzer and Simonin (1996) as:

$$\nu_g^t = \frac{2}{3} q_g^2 \tau_g^t \left[1 + C_{12} \frac{\alpha_k}{\alpha_g} \frac{\tau_{gk}^t}{\tau_{gk}^F} \left(1 - \frac{q_{gk}}{2 q_g^2} \right) \right]$$

where q_{gk} is the fluid-disperse phase covariance.

The effective stress tensor for disperse phase has two contributions as of the gas phase. The first contribution $\langle u_{k,i}' u_{k,j}' \rangle$ is the kinetic stress tensor that represents the transport of the momentum by the particle velocity fluctuations. The second one $\theta_{k,ij}$ is the collisional stress tensor that accounts for destruction and exchange of the momentum during inter-particle collisions. The constitutive equation of the effective stress tensor for the disperse phase is:

$$\Sigma_{k,ij} = \left[P_k + \lambda_k \frac{\partial U_{k,m}}{\partial x_m} \right] \delta_{ij} - \mu_k \left[\frac{\partial U_{k,j}}{\partial x_i} + \frac{\partial U_{k,i}}{\partial x_j} - \frac{2}{3} \delta_{ij} \frac{\partial U_{k,m}}{\partial x_m} \right]$$

The constitutive relations for viscosity and diffusivity are derived in frame of the extension of kinetic theory of dry granular flow and given by Balzer et al. (1996). The collisional pressure and the bulk viscosity are written as follows

$$P_k = \frac{2}{3} \alpha_k \rho_k q_k^2 \left[1 + 2\alpha_k g_o (1 + e_c) \right]$$

$$\lambda_k = \frac{4}{3} {\alpha_k}^2 \rho_k d_k g_0 (1 + e_c) \sqrt{\frac{2}{3} \frac{q_k^2}{\pi}}$$

with the disperse phase agitations q_p^2, the restitution coefficient e_c that determines energy loss during inter-particle collisions and g_0 is the pair correlation function. The shear viscosity is the linear combination of the collisional and the kinetic stress: $\mu_s = \alpha_k \rho_k \left[\nu_k^{kin} + \nu_k^{coll} \right]$

where

$$\nu_p^{kin} = \left[\frac{1}{3} \tau_{fp}^t q_{fp} + \frac{1}{2} \tau_p \frac{2}{3} q_p^2 (1 + \alpha_p g_0 \phi_c) \right] / \left[1 + \frac{\sigma_c}{2} \frac{\tau_p}{\tau_c} \right],$$

$$\nu_p^{coll} = \frac{4}{5} \alpha_p g_0 (1 + e_c) \left(\nu_p^{kin} + d_p \sqrt{\frac{2}{3} \frac{q_p^2}{\pi}} \right)$$

with $\sigma_c = \frac{1}{5}(1 + e_c)(3 - e_c)$ and $\Phi_c = \frac{2}{5}(1 + e_c)(3e_c - 1)$.

The collision stress of the effective stress tensor is not taken into account for the liquid phase.

The transport equations of particle agitation and fluid-particle correlations are beyond of this study, for further information, see Simonin (1996).

In the transport equation of the mass fraction of the liquid vapour, the correlation between gas phase and the mass fraction fluctuations is modelled as the diffusion and defined by $\langle y_p' u_{g,i}' \rangle = \frac{\nu_g^t}{Sc_t}$ with the Schmidt number Sc_t equal to 1.8.

Characteristic Time Scales

In the formulation of the transport equations, several characteristic time scales are defined. The time of interaction between disperse phases and gas phase fluctuations or the eddy-particle interaction time is defined by

$$\tau_{fp}^t = \frac{\tau_t}{Sc_t} \left[1 + C_\beta \xi_r^2 \right]^{-1/2} \quad \text{with} \quad \xi_r = |V_r| / \sqrt{\frac{2}{3} k}$$

where C_β is a constant equal to 1.8. Theoretically, it corresponds to the Lagrangian integral scale of turbulence seen by particles. The particle-particle collision time for the particulate phase is

$$\tau_p^c = \left(24 \alpha_p \frac{g_0}{d_p} \sqrt{\frac{2}{3} \frac{q_p^2}{\pi}} \right)^{-1}$$

where g_0 accounts for the increase of the probability of collisions as the suspension becomes denser. Lun and Savage (1986) proposed the correlation function for the distribution function as $g_o = (1 - \alpha_k / \alpha_{k,max})^{-2.5 \alpha_{k,max}}$ with a $\alpha_{k,max} = 0.64$ maximum random packing of an identical sphere particle suspension. These characteristic times scales are useful to determine the dominant mechanism in a suspension. The characteristic time scale of the convection/diffusion heat transfer is given by

$$\tau_{gk}^T = \frac{\rho_k c_{p,k}}{6 \lambda_g} \frac{d_k^2}{\langle Nu \rangle}$$

with $\langle Nu \rangle$ is the thermal conductivity of the gas phase. The Nusselt number of the dispersed phase is $\langle Nu \rangle = 2 + 0.6 \langle Re_p \rangle^{(1/2)} Pr^{1/3}$.

Flow Configuration

The grid was constructed by O-grid and it has approximately 220000 cells. The grid is uniform in direction x, y ($\Delta x = \Delta y = 0.06\,m$) with $\Delta z = 0.04\,m$ and we refined grid close to the injection. The computational grid is shown in Figure 3. The time step during the pre-injection of the bed as well as during the evaporation is typically about $\Delta t = 1 \times 10^{-5}\,s$ and the initial height of the bed is $3.4\,m$. During the evaporation, the gas and the droplets do not locally react when the size of the reactive particles is smaller than a given diameter (taken about $1\,\mu m$). The wall boundary condition with standard wall function accounting for the friction at the wall is used for the gas phase. For the particles and the droplets, no-slip boundary condition is used (Fede et al., 2009).

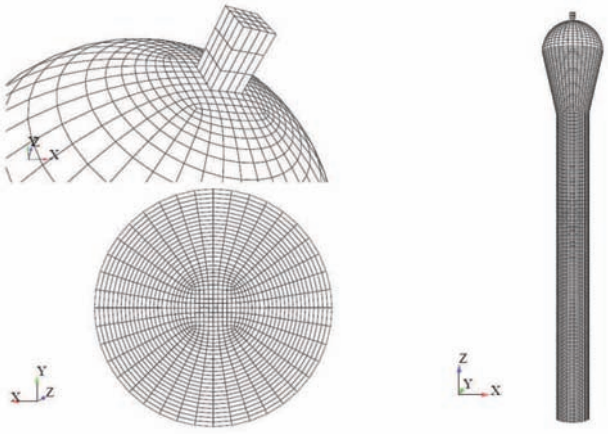

Figure 3: The computational domain.

Results and Discussion

The time evolution of the gas temperatures in the bed predicted by the simple model and the experimental at two locations are compared in Figure 4. We first modeled the wall as an adiabatic (the orange line). The temperature drop is overestimated as compared with the experimental data. Then, we set the heat transfer coefficient h_w to $320 W/m^2 K$ by using the following correlation

$$h_w = 0.86\frac{\lambda_g}{d_p^{0.5}}Ar^{0.39} + 0.86\frac{\lambda_g}{d_p}Ar^{0.15}$$

with the Archimedes number given by

$$\frac{g d_p^3 \rho_g(\rho_g - \rho_l)}{\mu_g}$$

and the gas specific heat capacity λ_g. The wall temperature was initialized to 97.5^oC before the injection (it is assumed that the bed is completely isolated from the ambient temperature). The evolution of the wall temperature is given by

$$m_w \lambda_w \frac{dT_w}{dt} = h_w S_w (T_b - T_w)$$

where m_w is the mass of the wall and with an assumption of a uniform distribution of the temperature through the wall. As compared with the results of the case with the adiabatic wall assumption, the temperature drop is slightly improved (the blue line) but far from the experimental data. The temperature evolution of the wall is also shown in Figure 4 by the curve "T-Paroi". It can be seen that the wall temperature is closer to the temperature measured by the probe (the curves Sonde T6 and Sonde T7) in terms of the value and the gradient. For the wall temperature, the smooth and progressive cooling can be explained by the progressive increase of the temperature gradient between the wall and the bed.

We carried out the second parametric study by modeling the wall with an infinite size. The results of the case with the infinite size and the heat transfer coefficient h_b equal to $320W/m^2K$ are compared with previous cases in Figure 5 (green). This extreme case cannot explain the difference between the experimental data and the results of the simple model. We cannot obtain any improvement of the result for the initial cooling part, but there is an influence of the size of the wall on the relaxation process ($t > 100s$). It is not presented here but an additional parametric study was performed with the simple model with a higher heat transfer coefficient h_w. The experimental temperature was retrieved by an appropriate value of h_w by tuning. However, its value is too high to be realistic and the smooth temperature decrease of the experimental data is never observed.

The gas temperature predicted by the multi-fluid simulation at the several locations is shown in Figure 6. The heat transfer coefficient was set $320W/m^2K$ and the wall temperature was 97.5^oC for the 3-D simulation. Conversely, the temperature evolution in the bed by the simple model and 3-D simulations shows a strong temperature variation at the beginning of the injection while the evaporation rate is maximal during this period (maximum of the temperature gradient between liquid and gas and minimum of the vapor density). However, this trend is not obtained by the experimental and as the temperature at the probe is close to the temperature of the wall. We suspect that the value measured by the probe may be influenced by the thermal inertia of a solid media such as probe cover or the wall.

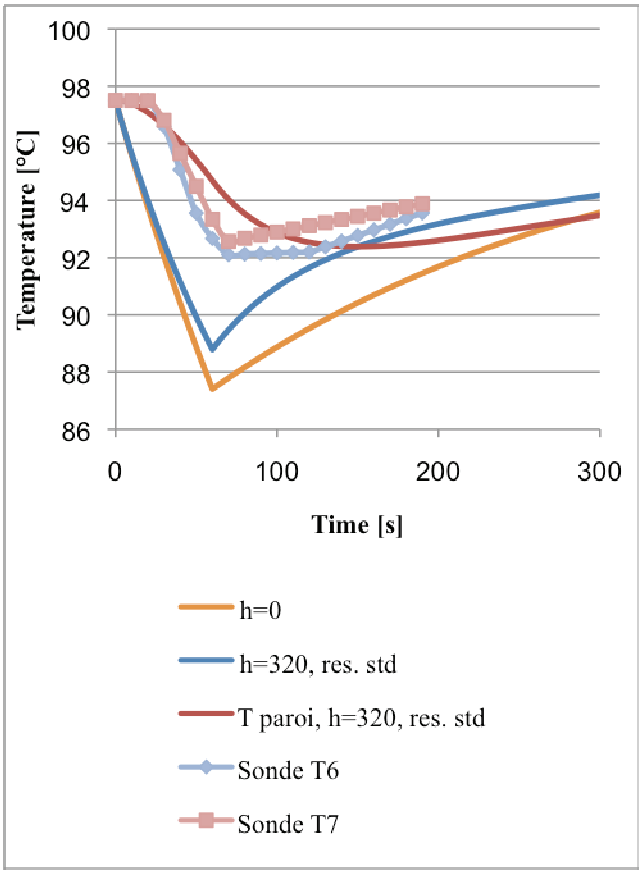

Figure 4: The time evolution of the gas temperature predicted by the simple model with an assumption of an adiabatic wall and accounting for the carbon steel and the experimental at two locations.

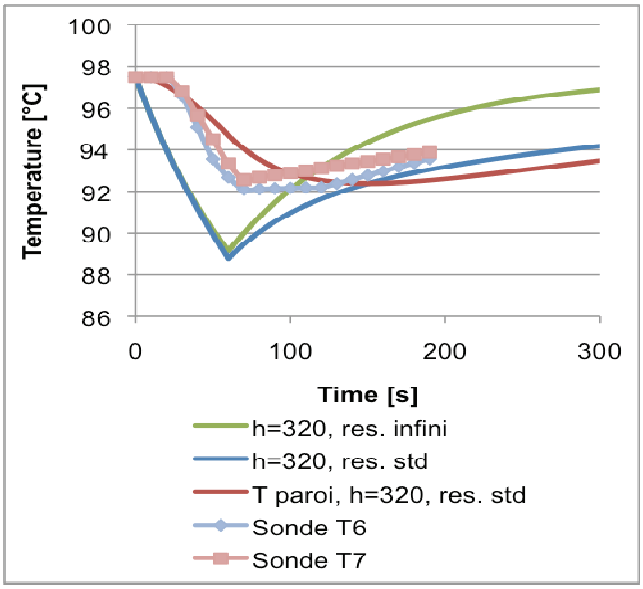

Figure 5: The time evolution of the gas temperature predicted by the simple model with accounting for the carbon steel and with infinite wall length and the experimental at two locations.

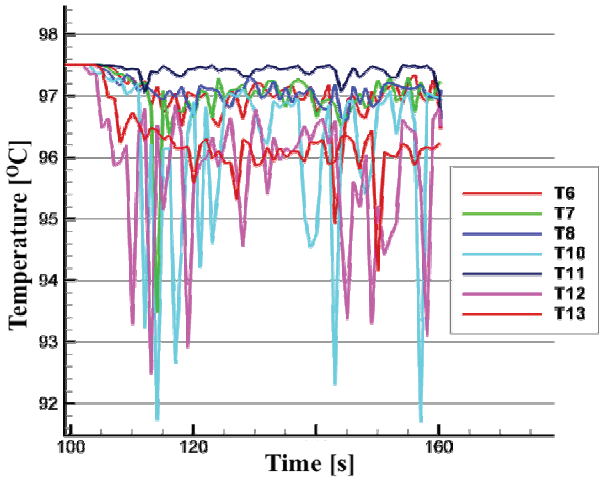

Figure 6: The time evolution of the gas temperature predicted at several locations by 3-D simulation with the heat transfer coefficient of $h_w = 320 W/m^2 K$ and the wall temperature of $97.5^o K$.

Conclusion

The time evolution of the gas temperature in an anisothermal dense fludized bed with a liquid injection is investigated by a simple model and 3-D Eulerian-Eulerian simulation. The simple model assumes the uniform distribution of solid and temperature in the bed and the results of this model are in a good agreement with the experimental data provided by INEOS. Additionally, results show that the wall-to-bed heat transfer has crucial effect on the time evolution of the gas temperature. For 3-D numerical simulation, we take into account the wall-to-bed heat transfer with the heat transfer coefficient h_w that is based on the parametric studies of the simple model. The simulation shows that the liquid evaporates quickly and the temperature is in a satisfactory agreement with the experiment data.

Acknowledgements

This work was granted access to the HPC resources of CINES under the allocation 2010-026012 made by GENCI (Grand Equipement National de Calcul Intensif) and of CALMIP under the allocation P0111 (Calcul en Midi-Pyrénées <spip.php?article282>)

References

Ariyapadi, S., Holdsworth, D.W., Norley, C.J.D., Berruti, F., Briens, C., 2003. Digital x-ray imaging technique to study the horizontal injection of gas-liquid jets into fluidized beds. International Journal of Chemical Reactor Engineering , Volume 1, Issue 1, 1542-6580.

Balzer, Böelle and Simonin] Balzer, G., Böelle, A., Simonin, O., 1995. Eulerian gas-solid flow modelling of dense fluidized bed, in: FLUIDIZATION VIII, Proc. International Symposium of the Engineering Foundation, pp. 409–418.

Bruhns, S., Werther, J., 2005. An investigation of the mechanism of liquid injection into fluidized beds. AIChE Journal 51, 766– 775.

Gobin, A., Neau, H., Simonin, O., Llinas, J.R., Reil- ing, V., Selo, J.L., 2003. Fluid dynamic numerical simulation of a gas phase polymerization reactor. International Journal for Numerical Methods in Fluids 43, 1199–1220.

He, J., Simonin, O., 1993. Non- equilibrium prediction of the particle phase stress tensor in vertical pneumatic conveying, in: ASME FED Gas Solid Flows.

House, P.K., Saberian, M., Briens, C.L., Berruti, F., Chan, E., 2004. Injection of a liquid spray into a fluidized bed: Particle-Liquid mixing and impact on fluid coker yields. Industrial & Engineering Chemistry Research 43, 5663–5669.

Konan, N.A., Neau, H., Simonin, O., Dupoizat, M., Geaziou, T.L., 2010. 3D unsteady multiphase simulation of uranium tetrafluoride particle fluorination in fluidized bed pilot, in: Yue, G., Zhang, H., Zhao, C., Luo, Z. (Eds.), Proceedings of the 20th International Conference on Fluidized Bed Combustion. Springer Berlin Heidelberg, pp. 1152–1158.

Kunii, D., Levenspiel, O., 1991.Fluidization Engineering, Butterworth-Heinemann Series in Chemical Engineering, Boston.

Simonin, O., 1991b. Prediction of the dispersed phase turbulence in particle-laden jets, in: Proc. 4th Int. Symp. on Gas-Solid Flows, ASME FED, pp. 197–206.